
Faculty of Science

Faculty Publications

This is a post-review version of the following article:

Sulphide-sulphate stability and melting in subducted sediment and its role in arc mantle redox and chalcophile cycling in space and time

Dante Canil, Steven A. Fellows

2017

The final published version of this article can be found at:

<https://doi.org/10.1016/j.epsl.2017.04.028>

Citation for this paper:

Canil, D. & Fellows, S.A. (2017). Sulphide–sulphate stability and melting in subducted sediment and its role in arc mantle redox and chalcophile cycling in space and time. *Earth and Planetary Science Letters*, 470, 73-86.

<https://doi.org/10.1016/j.epsl.2017.04.028>

**Sulphide-sulphate stability and melting in subducted sediment and its
role in arc mantle redox and chalcophile cycling in space and time**

Dante Canil^{1*} and Steven A. Fellows^{1,2}

1. School of Earth and Ocean Sciences, University of Victoria, Victoria, B.C.

V8W 3P6 CANADA

2. Present address: Department of Earth Science, Utah Valley University

Orem, Utah, 864058 USA

*Corresponding author: dcanil@uvic.ca

Abstract

The redox budget during subduction is tied to the evolution of oxygen and biogeochemical cycles on Earth's surface over time. The sulphide-sulphate couple in subducted crust has significant potential for redox and control on extraction of chalcophile metals from the arc mantle. We derive oxygen buffers for sulphide-sulphate stability ('SSO buffers') using mineral assemblages in subducted crust within the eclogite facies, and examine their disposition relative to the fO_2 in the arc mantle along various P-T trajectories for subduction. The fO_2 required for sulfide stability in subducted crust passing beneath an arc is shifted by variations in the bulk $Ca/(Ca+Mg+Fe)$ of the subducting crust alone. Hotter slabs and more Fe-rich sediments stabilize sulphide and favour chalcophile sequestration deep into the mantle, whereas colder slabs and calcic sediment will stabilize anhydrite, in some cases at depths of melt generation in the arc mantle (< 130 km). The released sulfate on melting potentially increases the fO_2 of the arc mantle. We performed melting experiments on three subducted sediment compositions varying in bulk $Ca/(Ca+Mg+Fe)$ from 0.3 to 0.6 at 2.5 GPa and 900-1100°C to confirm how anhydrite stability can change by orders of magnitude the S, Cu, As, Zn, Mo, Pb, and Sb contents of sediment melts, and their subsequent liberation to the arc mantle. Using Cu/Sc as a proxy for the behavior of S, the effect of variable

subducted sediment composition on sulfide-sulfate stability and release of chalcophiles to the arc mantle is recognizable in volcanic suites from several subduction zones in space and time. The fO_2 of the SSO buffers in subducted sediment relative to the arc mantle may have changed with time by shifts in the nature of pelagic sedimentation in the oceans over earth history. Oxidation of arc mantle and the proliferation of porphyry Cu deposits may be latter-day advents in earth history partly due to the rise of planktic calcifiers in the oceans in only the past 250 million years.

1. Introduction

The upper oceanic crust is overlain by a thin veneer of sediments, the bulk compositions of which are an integration of weathering, hydrothermal alteration, and biochemical processes in the oceans. Some chemical components of oceanic sediment are recycled by subduction into the mantle source region for arc magmas which rise, form new crust that weathers and erodes, completing the cycle (Tera et al., 1986; Plank 2005). The long-term impact of subducted sediment is recognizable in the geochemistry of mantle-derived magmas over time (Collerson and Kamber, 1997; Andersen et al, 2015) and is an important facet of the geochemical cycles for S, H, and C (Canfield 2004; Hirschmann and Dasgupta, 2009).

The recycling of S by subduction is particularly important for biogeochemical cycles, the history of degassing of magmas, and the transfer of ore metals to the crust. Oceanic sediment contains significant levels of S (Alt et al, 1992) and its release or sequestration during subduction may play a role in the redox of arc mantle and magmas (Evans, 2012), or control the deep earth S cycle over long time scales (Canfield, 2004). Sulfur isotopes in arc magmas suggest that subducted oceanic sediment is a likely and significant source for the S enrichment observed in arc magmas (Alt et al, 1993; de Hoog et al., 2001). Fluids or melt liberated from the subducted crust are efficient vectors for transport of S into the arc mantle (Evans, 2012; Jegu and Dasgupta, 2013; 2014; Tomkins and Evans, 2015). What is not known, however, is if the recycling and release of S and other chalcophile elements into the sub-arc mantle is controlled by the parameters of subduction, or the wide range of possible bulk compositions of oceanic sediments, both of which vary in modern settings and over geologic time.

The redox budget of subducted sediment and its potential for oxidation of the arc mantle is dictated by the abundance and the interplay of S, H, C and/or Fe (Evans, 2012). Sulfur is the smallest in abundance of these elements in subducting crust, but has a large oxidation power: one mole of S^{6+} can oxidize eight moles of Fe^{2+} to Fe^{3+} . Constraints on the subduction and release of S inform the debate of how the arc mantle can become oxidized (Parkinson and Arculus, 1999), or whether the redox state of arc magmas is imprinted in their source, or a product of their ascent and differentiation (Kelley and Cottrell, 2012; Lee et al, 2005; 2010). Reducing conditions in oceanic sediment would stabilize sulphide and sequester S for limited oxidation potential, whereas oxidizing conditions will stabilize sulphate, possibly causing greater release of S during subduction and mantle oxidation (Prouteau and Scaillet, 2013). The budget for other ore metals in the arc setting (Cu, Pb, Zn) would also be controlled by the stability of sulphide, their primary host (McInnes et al, 1999; Mungall, 2002).

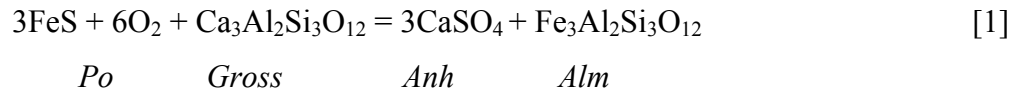
To this end, we first investigate how the bulk composition of oceanic sediments may control the stability of sulphide and sulphate during subduction. We then performed melting experiments on different oceanic sediment compositions at slab interface conditions to examine how the release of S or other chalcophiles is affected by redox state and sulphide stability, in scenarios where subducted sediments melt. Possible proxy signals on the cycling of S and chalcophile elements into the arc mantle are made evident using data from modern arcs in which the history of volcanism and incoming subducted sediment composition are known. We speculate how the mechanism for S recycling or arc mantle oxidation may have changed over earth history, due to shifts in the mode of carbonate sedimentation in the oceans over geologic time.

2. Sulphide - sulphate (SSO) oxygen buffers during subduction

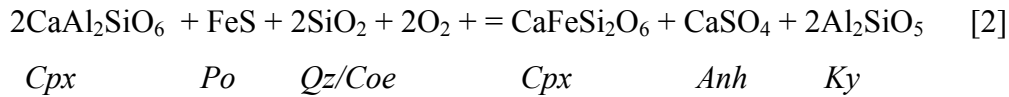
The total bulk composition of a given sedimentary column on the ocean floor varies broadly between Si-Al-rich or ‘pelitic’ and Ca-Mg carbonate-rich end members (Fig. 1) depending on sedimentation rate, proximity to continental sources, biological productivity in the ocean, and the preservation of carbonate or opal (Plank and Langmuir, 1998). The hosts for S in oceanic sediments are sulphate (anhydrite) precipitated from oxic ocean water and sulphide (pyrite or pyrrhotite) formed hydrothermally or by biogenic reduction of seawater sulphate (Alt et al., 1993; Canfield, 2004). The

concentration of sulphide or sulphate in oceanic sediments varies regionally, or even within the same sedimentary column (Alt and Burdett, 1992). Possible return pathways of S in these hosts to the mantle during subduction will be controlled by oxidation state (Prouteau and Scaillet, 2013).

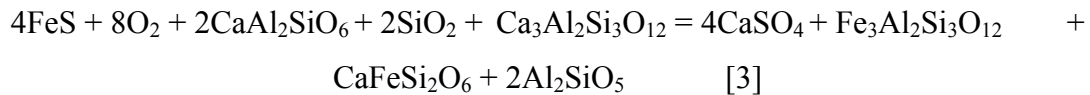
Experiments show that all oceanic sediment compositions, regardless of whether pelitic or carbonate-rich (Fig. 1), produce an eclogitic assemblage (clinopyroxene + garnet + quartz/coesite \pm phengite \pm kyanite) when subducted (Mann and Schmidt, 2015). To examine and quantify the effect of fO_2 on sulphide-sulphate stability in deeply subducted oceanic crust, we consider buffer reactions involving sulfides, anhydrite and the eclogite assemblage (clinopyroxene + garnet \pm kyanite \pm quartz/coesite). The first two are named ‘GAP’ (garnet-anhydrite-pyrrhotite):



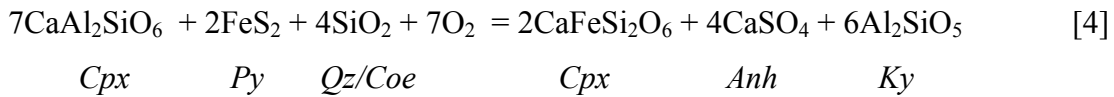
and ‘CAP’ (clinopyroxene-anhydrite-pyrrhotite):



These can be combined for clinopyroxene+garnet assemblages as ‘GCAP’:



Evidence from blueschists and eclogite terrains suggests the identity of the sulphide phase can be either pyrrhotite or pyrite during subduction at various metamorphic grades, though pyrrhotite is more common in metasediments at higher grades (Brown et al, 2014). Substitution of pyrite for pyrrhotite in [2] leads to the ‘CAPY’ reaction (clinopyroxene-anhydrite-pyrite):



Hereafter, we refer collectively to any of GCAP, GAP, CAP or CAPY [1-4] as the ‘SSO buffers’ in sediments at eclogite facies conditions.

Experimental data also show that the Ca and Fe components in garnet at eclogite facies conditions change with the bulk X_{Ca} (= molarCa/(Ca+Fe)) of subducted sediment compositions (Fig. 2). For this reason, the fO_2 of the GAP or GCAP buffer [1,3] at a

given P and T is expected to shift in oceanic sediments as a function of their bulk composition, due to changing the activities of Fe- and Ca- bearing components in the garnet phases with bulk composition. A similar shift in the CAP or CAPY [2,4] buffers is less obvious, however, because experimental data on sedimentary protoliths at eclogite facies conditions show that in clinopyroxene, the tschermak ($\text{CaAl}_2\text{SiO}_6 - \text{X}_{\text{CaTs}}$) component is typically low and varies little (< 0.05), and the hedenbergite ($\text{CaFeSi}_2\text{O}_6$) component is as strongly affected by T as by bulk composition (Fig. 2).

At a given P and T, the $f\text{O}_2$ of the SSO buffers in equations [1] to [4] can be calculated using an internally consistent thermodynamic database for all phases (Holland and Powell, 2005; Evans et al., 2010). To calculate activities of variable garnet compositions we applied a non-ideal asymmetric solution model for garnet. For a_{CaTs} and a_{Hed} of clinopyroxene in reactions [2,3,4] a symmetric non-ideal model was used with an assumed a Margules parameter ($W_{\text{CaTs-Hed}}$) of 25 kJ, similar in magnitude to that measured for Jadeite - Hed solid solutions (Wood, 1979; Holland, 1990). All other phases in [1] to [4] were assumed to be pure in composition except pyrrhotite. We assume a_{Po} of 0.875 (Newton and Manning, 2005). The use of either quartz or coesite affects results by less and 0.1 log $f\text{O}_2$ unit.

There are few experimental studies reporting the stability of Po, Py or Anh with garnet or clinopyroxene at known $f\text{O}_2$ with which to test the accuracy of our SSO buffers. The calculations for the GAP or GCAP buffer [reactions 1,2] can be tested independently using compositional data for garnet in S-bearing bulk compositions crystallizing Po or Anh with clinopyroxene+garnet \pm quartz/coesite. Jago and Dasgupta (2013, 2014) stabilized either Po or Anh in equilibrium with garnet in hydrous metabasalt at 800 - 1050°C and 2 - 3 GPa. Our GAP/GCAP model reproduces their experimental results to within 0.5 log $f\text{O}_2$ units (Fig 3). Prouteau and Scaillet (2013) partially melted hydrous pelite and basalt at 800-950°C and 2 – 3 GPa in the presence of garnet \pm Po or Anh. Our $f\text{O}_2$ values calculated using the GAP/GCAP equilibrium [reaction 1,2] satisfy the stability of Po in their experiments, but are ~ 1 log $f\text{O}_2$ unit lower than their single experiment stabilizing Po+Anh. Nevertheless, the $f\text{O}_2$ in the experiments of Prouteau and Scaillet (2013) was estimated using a solution model for H_2O in silicate liquids with uncertainty

of at least $\pm 0.5 \log fO_2$ units. We thus assume our GAP buffer is accurate to $\pm 0.5 \log fO_2$ units.

Application of reactions [1] to [4] to examine sulphide-sulphate stability in sediments with depth in various bulk compositions also requires knowing the P-T trajectory of crust during subduction. Subducted slabs can have a range in T at depth along their interface with the mantle, depending on the rate, geometry and age of subduction (Syracuse et al, 2010; van Keken et al, 2011). Figure 4 shows temperatures from thermal models for the top of a slab of young hot crust superimposed on a compilation of P-T data from eclogites and blueschists produced by subduction. One conundrum is several of such thermal models are cooler than subduction zone rock temperatures by 50 – 150°C depending on pressure (Penniston-Dorland et al, 2015). To address these differences we assumed three P-T trajectories during subduction for our SSO buffer calculations. In two cases, we simply fit the middle and extremes in the blueschist and eclogite P-T array to define the interface of a ‘warm’ and ‘hot’ subducting slab with depth, respectively (Fig. 4). In a third case we use a ‘hot young slab’ thermal model (van Keken et al, 2012).

The effect of bulk sediment composition from high X_{Ca} ‘carbonate-rich’ to low X_{Ca} ‘pelitic’ on the fO_2 of the SSO buffers in reactions [1] to [4] for various slab interface temperatures is explored by changing the amount of Ca and Fe components in garnet or clinopyroxene. We varied X_{Ca} in garnet from 0.1 to 0.5, and X_{Hed} in clinopyroxene from 0.55 to 0.05, respectively - the exact range in composition in these minerals observed in experiments over the spectrum of X_{Ca} in sedimentary protoliths at subduction zone conditions (Fig. 2). The X_{CaTs} in clinopyroxene was held constant at 0.02, as observed in most of experiments at temperatures below 1100°C suitable for most slabs.

Given this variation in garnet and clinopyroxene compositions, the fO_2 of the SSO buffers [1] to [4] along a given P-T trajectory of subduction can be compared to that of the surrounding overlying arc mantle. We assumed the latter to be at FMQ (at the same P, T - Fig. 5) as evidenced by the fO_2 recorded by most arc mantle peridotites (Parkinson and Arculus, 1999; McInnes et al, 1999). *Although the fO_2 of the mantle decreases with depth ($\sim 1 \log fO_2$ unit/GPa – Miller et al, 2016) the latter constraint of FMQ is still regarded as a minimum for the upper mantle above a subducting plate, as shown by*

garnet peridotites exhumed from >90 km depths in this setting (~FMQ+2 - Malaspina et al, 2009). In light of the homogenization of fO_2 over tens of kilometer scales observed in metamorphic terrains and orogenic peridotite massifs (Ague et al, 2002; Harlov, 2012; Woodland et al, 2006) we assume this variable in subducted sedimentary crust equilibrates with the overlying mantle along the slab interface. If so, then sulphide is stable in the sedimentary protolith when the fO_2 of a given SSO buffer is greater than FMQ ($\Delta FMQ > 0$), and sulphate is stable when $\Delta FMQ < 0$. In our calculations this sulphide-to-sulphate transition varies with depth from ~ 110 – 180 km, depending on bulk sediment composition, slab temperature model, or the particular SSO buffer being considered (blue shaded area of Figure 5). For reactions [1-4] to ensue would require introduction of an oxidant to slab sediment, to change or sulphide to sulphate. This would require reduction of another element in sediment (Fe^{3+} , C^{4+}) or an open system, but seems plausible given the growing evidence for fluxes of CO_2 or SO_4 in fluids during metamorphism both in and outside the subduction zone setting (Ague and Nicolescu, 2014; Harlov, 2012; Pons et al, 2016).

The results for GAP and GCAP buffers (reactions [1,2]) are essentially identical, and show that for a given P-T trajectory of subduction, sulphide is more stable in low bulk X_{Ca} or ‘pelitic’ sediments throughout much of their subduction into the arc mantle. Sulphate is the stable phase in these compositions only at depths greater than about 140 km, notably below the range of depths to the slab beneath volcanic fronts in modern arcs (England and Katz, 2010). In contrast, carbonate-rich oceanic sediments with higher bulk X_{Ca} (Fig. 1) shift the SSO buffers to lower fO_2 (Fig. 5a) and stabilize sulphate in subducted sediment at shallower depths (110 - 125 km) within the depth region of arc magma generation. The depth for sulphide-sulphate transition varies with temperature of the slab and bulk composition. Comparison of Figures 5a and 5b shows that the ‘Vankeken’ and ‘warm’ slab temperature models produce results within uncertainty for the GAP and CAP buffers. In contrast, for a given SSO buffer, a ‘hot’ subduction zone stabilizes sulphide relative to sulphate to depths far below those to the slab (and magma generation) beneath most arc volcanic fronts (Fig. 5c). For a given bulk X_{Ca} of the protolith, the depth at which sulphide becomes unstable relative to sulphate in the CAP assemblage is slightly less than in GAP. Changing the identity the sulphide phase from

pyrrhotite to pyrite has a marked effect. The CAPY assemblage stabilizes sulphide (as pyrite) to much greater depths, and sulphate cannot be stabilized in this assemblage to depths of at least 180 km, far below the slab depths of volcanic fronts in arcs (Fig. 5d).

The uncertainties of $\pm 0.5 \log fO_2$ units in the SSO buffers [1 to 4] propagate to errors in absolute depths of the sulphide-sulphate transition in the slab sediments of 10 or 20 km. Nevertheless, the calculations are instructive in showing how potentially significant variations in sulphide stability in subducted sediments with depth ensue just by varying bulk composition, thermal parameters of subduction or the original identity of the subducted sulphide phase. Hot subduction, Fe-rich oceanic sediments (low bulk X_{Ca}) or those in which pyrite is the only stable sulphide phase tend not to stabilize sulphate at any depths relevant to arc magma generation. Colder subduction or calcic (high bulk X_{Ca}) sediments have the potential to produce sulphate at slab depths beneath arc volcanic front. These changes in sulphide stability could greatly affect how S is mobilized and recycled in subduction zones, if sediments partially melt or lose fluid in some scenarios, depending on age or geometry or other factors at a convergent margin. This is because S solubility in melts at sulphate-saturation is orders of magnitude higher than in the sulphide-saturated case (Scaillet et al, 1998; Jugo et al, 2005; Jugo, 2009). In this way, the GAP and CAP buffers allow predictions of whether S and chalcophile elements might be easily sequestered or released to the arc mantle wedge, depending on bulk sediment composition, and whether sediment melting ensues beneath an arc. To investigate this effect directly, we examined by experiment the behaviour of S and other chalcophiles in partial melts of oceanic sediments at eclogite facies conditions in the presence of either sulphide or sulphate.

3. Experiments

3.1 Starting Materials

On the basis of previous phase equilibrium studies we synthesized two starting compositions that represent the partial melts of end members of oceanic sediment bulk compositions (Fig. 1, Table 1). The GM composition replicates the partial melt of a pelitic global oceanic sediment analogue ('GLOSS') produced at 2.5 GPa and 900°C (Herman and Spandler (2008)). The TSC composition is a carbonate-rich hydrous

sediment composition similar to HPLC1 studied by Tsuno and Dasgupta (2011). The GM starting composition was synthesized by mixing reagent grade SiO_2 , TiO_2 , Fe_2O_3 , Na_2CO_3 , and K_2CO_3 in an agate mortar. The mixture was then decarbonated at 800°C . Gibbsite [$\text{Al}(\text{OH})_3$], portlandite [$\text{Ca}(\text{OH})_2$], and brucite [$\text{Mg}(\text{OH})_2$] were added as sources for water. The powdered mixture was shaken in a plastic canister for 15 minutes and ground under ethanol in an agate mortar for 15 minutes. This process was repeated three times to ensure homogeneity. The GM composition was then split, with 2 wt.% natural anhydrite added to one split (GM-an), and 2 wt.% natural pyrite added to the other (GM-py) producing two differing starting redox states for S at levels predicted to maintain sulphide or sulphate saturation (Prouteau and Scaillet, 2013). The GM compositions were doped with trace elements (Sc, Cu, Zn, As, Sr, Nb, Mo, Sb, Ba, La, Ce, Yb, Pb, Th, and U) in 100-250 ppm concentrations added as a cocktail of NIST certified trace element solutions (Table 1). The doped powder was then dried under a heat lamp, mixed again in a plastic canister for 15 minutes and ground in an agate mortar for further 15 minutes. This process was repeated three times to homogenize the trace elements into the composition. The TSC-py and TSC-an starting compositions was synthesized using a similar method to GM but with CaCO_3 , Na_2CO_3 , and K_2CO_3 added as sources of CO_2 .

3.2 Experiments

The melting experiments were carried out in an end-loaded piston-cylinder apparatus at 2.5 GPa over a range of temperatures (700 to 1100°C) chosen to intersect various P-T trajectories for subducted crust (Fig. 4; Table 2). We employed 13 mm CsCl assemblies, with a pressure calibration and the hot-piston out method as described in Canil (1999). To explore the effect of $f\text{O}_2$ the experiments were carried out under oxidizing and reducing conditions. For the oxidizing experiments the pyrite-bearing and anhydrite-bearing starting material were placed inside of separate 3mm Au capsules and welded. The two Au capsules were then packed into a 4mm Pt capsule, filled with $\text{Al}(\text{OH})_3$. The $\text{Al}(\text{OH})_3$ breaks down at the experimental conditions to ensure H_2O saturation during the experiments and obviate H_2O -loss from the inner Au capsules (Fig. 6). The reduced experiments were carried out using the same method as above but with the addition of powdered graphite on the bottom and top of the starting material in the Au capsules before welding. The outer 4mm Pt capsule was filled with $\text{Al}(\text{OH})_3 + \text{C}$ to ensure more

reducing conditions were maintained in the experiment. For each experiment, the charges were heated to the run temperature, held for up to 48 hours, and then quenched in seconds by cutting power to the furnace assembly.

3.3 Analytical Methods

Experimental products were mounted in epoxy and polished for analysis. Polished sections were examined by reflected light microscopy and by scanning electron microscopy (SEM) using a Hitachi S-4800 scanning electron microscope (SEM). Major element concentrations in each phase and the glass were determined using a CAMECA SX50 electron microprobe (EMP) at the University of British Columbia at a 15 kV acceleration voltage and a beam current of 20 nA, and peak counting times of 20 seconds. The beam diameter was 1 μm for mineral analyses and defocused to 40 μm for glass analysis.

Trace elements (Li, S, Sc, V, Co, Cu, Zn, As, Sr, Nb, Mo, Sb, Ba, La, Ce, Yb, Pb, Th, U) in the glass from the run products were measured by laser ablation inductively coupled mass spectrometry (LA-ICPMS) after the procedures described in Fellows and Canil (2012). The 213 nm Nd-YAG laser was fired at 10 Hz using a power of ~ 0.400 mJ and a fluence of 30.5 J/cm^2 with spot sizes of 20–40 μm depending on the sizes of glass regions. Results on BCR2g standard for all trace elements (Table 3) are within 8% of the reference values except for Zn (25%). We measured 112 ± 126 ppm S on BCRg, within the results and precision of 158 ± 126 ppm reported by Shu and Lee (2015) for the same glass. The time resolved spectra of run product glasses were carefully screened to eliminate contamination from small crystals. Only spectra with consistent and anomaly-free profiles were selected. For experiments with small and/or few melt pools for analysis, the epoxy mount was analyzed by LA ICPMS and then re-polished deeper to expose new melt regions in the capsule for subsequent analysis.

4. RESULTS

4.1 Experimental Products

All experiments contained silicate glass and a free fluid phase as evidenced by the presence of vesicles in glass (Fig. 7). Given the low experimental temperatures, crystalline phases were mostly $< 10\text{--}15 \text{ }\mu\text{m}$. Depending on the starting bulk composition

and experimental conditions the crystalline phases observed were clinopyroxene, phengite, K-feldspar, kyanite, garnet, quartz, anhydrite, pyrite, rutile, magnetite, biotite, and titanite (Table 2). Run products for both starting compositions (GM and TSC) contain clinopyroxene, titanite, magnetite, rutile, and K-feldspar and are typically sub-euhedral (Fig. 7). Quartz, calcite, garnet, and pyrrhotite were subhedral. Phengite and kyanite were primarily needle-like, bladed, or platy. When present, anhydrite was anhedral and ragged in appearance, but may have suffered from plucking and dissolution during the polishing stage. Kyanite, magnetite, anhydrite, rutile, and garnet proved to be difficult to analyze due to their small size, crystal habit, or were obscured by intergrowth with other phases. Small globules of immiscible calcite (melt?) were also recognized, similar to the features noted in sediment melting experiments (Skora 2015; Mann and Schmidt, 2015).

Glass could be analysed in all but two experiments (Table 3). Mineral compositions are given in E-Appendix A. The phase proportions in each experiment could not be obtained by mass balance due to the presence of several mineral phases that were frequently too small or clustered to be reliably analysed by EMP. The inability to analyze all minerals and mass balance in many experiments does not change the overarching purpose of the experiments, which was to examine chalcophile elements in the melt phase.

4.2 Equilibrium

We carried out a time series to test for equilibrium in experiments at 900 °C over 6, 24 and 48 hours. The concentration of Cu, Zn, and As in the glasses at 24 h are within uncertainty of those for ~48 hours, suggesting equilibrium was reached by 24 hours (runs p403, p404, p405 - Table 3). We carried out the majority of our experiments for more than 45 hours, to ensure equilibrium.

4.3 Oxidation State of Experiments

Maintaining the presence of sulphide or sulphate in each experiment was central to the study and required some knowledge of the fO_2 , which is not straightforward in volatile-bearing experiments in a piston-cylinder device. Sources of oxidation are the dissociation of H_2O ($2H_2O = 2H_2 + O_2$) inside the inner Au capsule, and the presence of essentially all Fe as Fe^{3+} in the starting material. The oxidizing potential of the aforementioned sources

in the starting materials tended to stabilize sulphate. To stabilize S as sulphide (as pyrrhotite) in experiments, the disseminated C added to the inner and outer Au capsules served as a reductant that buffers the fO_2 to near CCO ($2C + O_2 = 2CO$), which lies 1.1 log units below the FMQ buffer at conditions of our experiments (Ulmer and Luth, 1990). The effectiveness of these approaches can be seen in the experimental run products. In the reducing graphite-bearing experiments, the anhydrite loaded in the one capsule would be reduced to pyrrhotite. Conversely, in the graphite-free experiments, the sulphide-bearing starting material is oxidized such that both capsules contained only anhydrite (Table 2).

We also applied the CAP and GAP buffer calculations (reactions [1 – 4]) to any run products containing clinopyroxene and in one case coexisting garnet that could be analysed by EMP. One caveat is that our run products contained either pyrrhotite or anhydrite, and never both. Thus, in the case of anhydrite-saturated experiments the calculated fO_2 from GAP or CAP is a minimum, whereas in pyrrhotite-saturated experiments the fO_2 is a maximum (Table 2). [Additionally some of our experiments did not contain kyanite present in the CAP buffer reaction.](#) Nevertheless, the application of the CAP and GAP methods allow some approximation that the fO_2 of at least some of the experiments from below FMQ to above FMQ+2 in pyrrhotite - and anhydrite -saturated experiments, respectively (Table 2).

4.4 Melt Compositions

Melts produced are broadly granitic in terms of Na_2O+K_2O (5 – 10 wt%) and SiO_2 (70-75 wt%) on an anhydrous basis, similar to those from previous sediment melting studies (summarized in Mann and Schmidt, 2015; Schmidt, 2015). The H_2O contents of melts are between 7 to 12 wt%, assuming the ‘by-difference’ method (difference in analytical total by EMP from 100%). Melts derived from the two different starting materials are mostly similar except for higher concentrations of CaO (2-3wt%) and FeO (1-2 wt%) in those from the more carbonate-rich TSC composition (Table 3).

The most striking result from the experiments is the difference in chalcophile metal concentration in sediment melts at different fO_2 conditions. The levels of S determined by LAICPMS vary from 60 to 4000 ppm, and though not very precise, are markedly higher in anhydrite-saturated experiments (Fig. 8a). The behaviour of S is

consistent with previous studies that suggest hydrous oxidized sediment melts favour sulphate dissolution and overall higher solubility of S (Scaillet et al., 1998; Prouteau and Scaillet, 2013; Jago and Dasgupta, 2014).

The concentration of Cu, Zn, As, Pb, Sb varies up to two orders of magnitude in melts with fO_2 increasing from below FMQ to near FMQ+2 (Fig. 8bc). This large difference occurs in both the GM and TSC starting compositions, regardless of whether the S was initially added as sulphide or sulphate to the starting material, and is dictated by the presence or absence of the former phase in the final run products.

When normalized to abundances in the starting material, Ba, Th, Nb, La, Ce, Yb and Sc showed slightly variable concentration in the melt, depending on the presence of coexisting K-feldspar or clinopyroxene, which would partition some of these elements differently. In oxidized experiments the chalcophiles (Cu, Zn, As, Pb, Sb) were strongly partitioned into the liquid, and in the same magnitude as the lithophile elements (U, Sr, Ba, Th, Nb, La, Ce, Yb), but showed extreme depletion in the melt in reduced experiments containing pyrrhotite (Fig. 9). All chalcophiles show strong positive correlations with one another, but there is differential partitioning, with some fractionation of Cu from Mo (Fig. 9). There is notable fractionation of Cu and Sc, and Ce from Pb depending on pyrrhotite versus anhydrite saturation. These element trends can be applied to examine the role if any for sediment melting and chalcophile element behaviour in the sources of arc magmas.

5. Discussion

5.1 Sediment melting and release of chalcophiles to the arc mantle

There are several lines of evidence for a sediment contribution to the source of arc magmas (Plank and Langmuir, 1993). Even small sediment contributions (3 – 6%) explain some isotope and element ratios (Th/La) in arc magmas (Elliot et al, 1997; Plank, 2005). Whether slab interface temperatures are hot enough to partially melt sediment is debated (Cooper et al, 2012; Behn et al, 2012). Some models suggest that temperatures along the interface of even the hottest slabs will not approach the lowest, H₂O-saturated melting point of oceanic sediments (Figure 4). A survey of P-T work on eclogites, however, calls some of these models into question (Penniston –Dorland et al, 2015). In

addition, the trace element abundances of eclogite facies rocks with metasedimentary protoliths show patterns consistent with retention by accessory phases to temperatures of $> 1050^{\circ}\text{C}$ - far above the slab interface temperatures in most subduction models (Behn et al, 2012). This observation has led to a model that, due to their lower density, slab sediments rise buoyantly as diapirs into the sub-arc mantle and partially melt (Gerya and Yuen, 2003; Behn et al, 2012; Marchall and Schumacher, 2012).

Whether sediment melting proceeds along the slab interface, or within buoyant diapirs, in what follows we assume that the outcome is partial melts imprinting sedimentary signatures on the arc mantle source region. Interaction and mixing of such hydrous sediment melts maintains saturation in olivine+orthopyroxene (Mallik et al., 2016). The bulk composition of the oceanic sediment and the temperature of the slab exert control on the SSO buffers with depth during subduction (Fig. 5). When sulphide is destabilized in the subducted sediment, marked introduction of S and chalcophile elements (Cu, Zn, As, Pb, Sb) from melted oceanic sediment to the arc mantle would ensue as shown by our experiments (Figs. 8, 9). The sulphate-rich sediment melts could also oxidize the mantle wedge directly as the S^{6+} in melt interacts with and destabilizes surrounding mantle sulphides, liberating additional chalcophile elements stored within them. Because subduction is a continuous process during the lifetime of an arc, the delivery of sediments of the same composition could buffer sulphide-sulphate stability and dictate the release or sequestration of S and chalcophiles to the mantle. Conversely, any changes in subduction parameters or the composition of subducted sediment beneath an arc over its lifetime may shift the SSO buffers, and alter the delivery of S and chalcophiles. We now test these predictions using erupted products in arcs that have varied subduction parameters or sediment compositions in space and time.

5.2 Nicaragua

Sediment subduction has had long history of study in the context of the chemistry of arc magmas. The Central American arc has in particular shown significant along strike variations in its chemistry that correlate with the composition and or extent of sedimentary input (Patino et al, 1990). Sedimentary input is particularly acute in Nicaragua, as shown by isotopes and trace elements in magmas erupted in this segment of the arc (Tera et al, 1986; Plank et al, 2002).

Nicaragua is also an ideal location to study the temporal changes in subducted sediment input, [as trenchward migration of the arc exposes volcanic rocks erupted over the past 20 m.y.](#) During this time period there has also been a profound change in the composition of sediments delivered to the arc. Changes in currents and upwellings between 20 and 10 Ma altered the carbonate compensation depth, leading to a sudden change from dominantly Ca-rich pelagic ‘carbonate ooze’ sedimentation on the subducting Cocos plate between 20 – 10 Ma, to a ‘carbonate crash’ and precipitation of mainly diatomaceous (Ca-poor) sediments after 10 Ma (Plank et al., 2002). The bulk X_{Ca} (= molar $Ca/Ca+Fe+Mg+Mn$) of sedimentary sections in several ocean drilling locations on the Cocos plate over this time period document a change in X_{Ca} from ~ 1.0 to < 0.2 after the ‘carbonate crash at 10 Ma (Plank et al., 2002). This change in X_{Ca} correlates directly with the mass of $CaCO_3$ in the sediments - from nearly 100 wt% pre-10 Ma, to less than 10% thereafter.

We can examine if this marked change from subduction of Ca-rich to Ca-poor sediments affected the SSO buffers in the slab, and is reflected in the chalcophile element systematics in the Nicaraguan arc magmas over the past 20 m.y. In this exercise we use Cu/Sc as a proxy for S during arc mantle melting for a number of reasons. Analysis of bulk S in many igneous rock suites is uncommon, and is often affected by degassing or surface weathering relative to Cu, even in relatively fresh lavas (Lee et al, 2012; Shu and Lee, 2015). Copper is similarly chalcophile but more commonly measured in rocks than S, but both of these elements along with Sc have broadly similar partition during mantle melting (bulk D mantle/melt ~ 0.1 -0.5) except when sulphide is present (Lee et al, 2012). The experimental data from this study confirm this behaviour is maintained even for partial melts of sediments (Fig. 9).

Figure 10 shows the Cu/Sc of lavas from the Miocene Nicaraguan arc plotted against their location relative to the modern Central American trench. The samples are filtered to consider only samples with less than 60wt.% SiO_2 , to avoid fractionation effects on the Cu/Sc ratio (Jenner et al, 2010; Lee et al, 2012). The age span of the Nicaragua lavas plotted in Figure 10 is about 10 to 7 Ma, spanning the time period for the ‘carbonate’ crash recorded by sediments on the incoming Cocos plate. Also shown in Figure 10 is the concentration of $CaCO_3$ in incoming sediments, whose absolute ages

vary from 20 to 0.45 Ma (Plank et al, 2002), but are here plotted where they would be in coordinates relative to the modern trench, assuming an incoming plate velocity of 8.5 mm/year (Horne et al, 2008). The sediment compositions are shown in this coordinate space so that their age-location is in the same plate reference frame as the arc lavas to which they are being compared. Plate velocities of the Cocos plate vary with latitude (deMets et al, 2010), and could surely have changed over the last 20 Ma, shifting absolute value of the points on Figure 10, but this would not change the age/location of sediment and lava compositions relative to one another.

We note a coincidence of the changing CaCO_3 recorded in incoming subducted sediments due to the ‘carbonate crash’ with an increase in Cu/Sc of the lavas. The Cu/Sc in volcanic rocks increases from ~ 2 to 9 with decreasing distance to modern trench, over a time period from 10 Ma to 7 Ma. *If subduction of sediments to the arc source region were instantaneous, the Cu/Sc in arc lavas in Nicaragua do not correlate with X_{Ca} of incoming sediment.* The arc front is typically 100 km from the trench, however, and so there is a time lag between subduction of sediment and its involvement in the source of arc magmas of at least a few million years. Thus, one explanation of the trend in Figure 10 is that pre-10 Ma, the subduction of Ca-rich sediments has destabilized sulphide at the depths of magma production beneath the arc volcanic front, as predicted by the shift of SSO buffers with bulk X_{Ca} (Figure 5). Between 20 and 10 Ma, subducted sediment is Ca-rich ($>90\% \text{ CaCO}_3$, $X_{\text{Ca}} > 0.95$) and sulphide is unstable at slab depths beneath the arc volcanic front, promoting release of Cu and related chalcophiles into the arc source, whether by direct melting of those sediments or by the diapir mechanism. After 7 Ma, incoming sediment entering the arc mantle source would be Ca-poor ($< 10\text{wt}\% \text{ CaCO}_3$, $X_{\text{Ca}} < 0.2$) and sulphide again is stabilized in the slab due to the lower bulk X_{Ca} (Figure 5), sequestering Cu relative to Sc as predicted by the experimental data (Fig. 9). Indeed, the eventual return to low Cu/Sc values (~ 3) in the modern arc is expected given the recent subduction of Ca-poor sediments. The systematics of chalcophile elements in the Nicaraguan arc, where sediment and lava compositions are well constrained in time and space, is wholly consistent with the shift in sulphide-stability with sediment composition predicted by the SSO buffers.

5.3 Global Trends in Arcs

We can extend the above observations on the well-studied Nicaraguan arc to a much coarser scale in all arcs globally. Sedimentary sections on oceanic plates entering subduction zones have been sampled by ocean drilling and compiled by Plank and Langmuir (1998). The bulk compositions of such sedimentary sections have been assembled from many lines of data to compare with arc geochemistry of arc magmas. One uncertainty is that not every sedimentary section has been measured directly at the trench, and several million years of subduction ensue between what is sampled on an incoming plate today and what is erupted in the modern arc. Nevertheless, examination of such data has been informative of the contribution of sediments to the source of arc magmas globally (Plank and Langmuir, 1998; Plank 2005). In this context we examine if there is a global signature of incoming arc sediment composition in chalcophile elements released in the arc as predicted by our SSO buffer calculations and our melting studies.

The bulk X_{Ca} of sediment sections for 14 modern trenches from the data given in Plank and Langmuir (1998) is compared with a compilation of Cu/Sc in volcanic rocks from their corresponding arcs. The latter data are compiled from 249 literature sources, with only post-1980 whole rock analyses by XRF or ICPMS methods being considered (<http://georoc.mpch-mainz.gwdg.de/georoc/> - references given in Elec Appendix B). Rocks were screened to consider only samples containing < 60 wt% SiO₂, to obviate any fractionation effects on Cu/Sc (Lee et al 2012). After applying these filters to the data, the total number of analyses is 3650 but varies in each arc depending on data availability and rock compositions (E Appendix C).

Despite the uncertainties in such a generalized global comparison, there is a remarkable correlation of X_{Ca} of trench sediment with Cu/Sc in volcanic rocks of modern arcs (Fig. 11). The changes observed in global arcs cannot simply be due to different bulk Cu in the subducted sediments delivered to the arc because the latter does not correlate with X_{Ca} (Fig. 1). The correlation Cu/Sc in arc magmas with X_{Ca} of trench sediment can be fit to a linear relationship with an $r^2 = 0.77$. A far better fit, however, is obtained using the following relation $y = 1/[1+10^{(a-bx)}]$, (where a and b are constants), which is the form of the equation describing S solubility in melts with a change in S speciation from S²⁻ (sulphide) to S⁶⁺ (sulphate) with increasing fO_2 (Carroll and Rutherford, 1987; Scaillet et al, 1998; Jugo, 2009). In a similar way, the change of Cu/Sc (our proxy for S) in the arc

magma reflects a shift in S speciation (from S^{2-} to S^{6+}) in melts or fluids delivering Cu to the arc source, the latter dictated by the effect of X_{Ca} of slab sediment on the nature of S-bearing phase stable (sulphide vs. sulphate) at depth beneath the arc. This could be investigated by further experimentation.

5.4 Deep earth S and chalcophile cycling over geologic time

The range in X_{Ca} observed for various modern convergent margin sediments (Fig. 1, Fig. 11, E Appendix C) is due to the diverse regional distribution of calcic pelagic sediments ('calcareous ooze') in the ocean basins (Ridgwell and Zeebe, 2005). The correlation of Cu in many modern arcs globally might be consistent with the variations in X_{Ca} of incoming subducted sediment affecting chalcophile release in arc sources (Figure 5), but this mechanism may have varied over geologic time. Planktic calcifiers, the main component of widespread calcic pelagic sedimentation in the deep modern oceans, are only a relatively recent biological revolution. Prior to only 250 m.y. ago, carbonate sedimentation in the oceans was mostly neritic (Ridgwell and Zeebe, 2005) and calcic pelagic sediment subduction may not have modulated chalcophile element cycles and arc oxidation at all. Alternatively, carbonate saturation gradients could have been even more homogeneous and uniform in an anoxic ocean prior to 500 m.y. ago (Higgins et al, 2009).

The occurrence of diamonds containing sulphides with mass independent S fractionation supports subduction of S into the mantle since the Archean (Farquhar et al, 2002). If it occurred, hot subduction may have been the norm in the Archean (VanHune and Moyen, 2012). The Archean oceans were sulfidic and Fe-rich (Canfield, 2004) and marine sediments subducted would have been Fe-rich. Those attributes would affect the SSO buffers in subducted sediment so as to cause marked sequestration of S, Cu and other chalcophiles from the arc mantle in the Archean. We tested this possibility by comparing Cu/Sc in Archean and modern volcanic rocks. We compiled only analyses published post-1980, and screened to contain < 60 wt% SiO_2 , again to obviate any fractionation effects on Cu/Sc. Komatiites were omitted, as they are possibly plume-related. After filtering for all analyses with $Ti/V < 20$ to identify rocks from the arc setting (Shervais, 1982), 222 Archean basalt analyses fit these criteria (E-Appendix C).

An important caveat of this exercise concerns the mobility of Cu during metamorphism in almost all volcanic rocks in the geologic record. Many Archean basalts

erupted subaqueously and have been altered during emplacement or regional greenschist facies metamorphism. Both these processes tend to deplete the rock in Cu by about 10% relative to the less mobile elements like Sc (Gregory, 2006; Patten et al, 2016). In this way, the Cu/Sc of Archean metabasalts in our comparisons might be considered minima.

The Cu/Sc in modern arc whole rocks and submarine glasses is significantly higher, on average, and more variable than that of MORB (Fig. 12, E-Appendix C), mirroring the S abundances in these same two settings (deHoog et al, 2001; Wallace, 2005). In contrast, Archean arc basalts have a mean Cu/Sc similar to MORB, and significantly lower than that of modern arc whole rocks or glasses (Fig. 12). This could be an artifact of the depletion of Cu in Archean rocks by seafloor or regional metamorphism described above. The more critical difference, however, is the markedly lower variance in the Cu/Sc of Archean arc basalts compared to modern ones, shown visually by less skew to high values (Fig. 12) and demonstrated statistically through an F-test ($F=3.92$, $p<0.0001$). The larger variance and skew to high Cu/Sc in modern arc magmas is consistent with the effect of subduction of Ca-rich sediments on the SSO buffers, leading to transfer of significant S and Cu into many modern arc mantle source regions. In the Archean case, this mechanism may have been suppressed or absent. It may be no coincidence that porphyry Cu deposits have considerable frequency in the Mesozoic and younger times, but show a paucity prior to then (Cooke et al., 2005). Prevalent oxidation and the release of chalcophiles to the mantle source of arcs forming porphyry deposits may ultimately have awaited the latter-day advent of planktic organisms raining down on to Earth's ocean floor in only the past 250 m.y. A more rigorous and comprehensive examination of Cu abundances in arc basalts over geologic time will be able to further address this conjecture.

Acknowledgements - We are grateful to J. Spence and M. Raudsepp for assistance with LA ICPMS and EMP analyses, respectively. We thank T. Lacourse for help with statistical analysis, and L. Coogan and P. Hoffman for suggestions. We especially thank K. Evans and H. Williams for their extremely helpful reviews of our paper. This research was supported by a NSERC of Canada Discovery Grant to DC.

References

- Ague, J.J., Baxter, E.F., Eckert Jr., J.O. 2002. High fO_2 during sillimanite zone metamorphism of part of the Barrovian type locality, Glen Clova, Scotland. *J. Petrol.*, 42, 1301-1320.
- Ague, J.J., Nicolescu, S. 2014. Carbon dioxide released from subduction zones by fluid-mediated reactions. *Nature Geosci.* 7, 355-359.
- Alt, J. Shanks III, W., Jackson, M.C., 1993. Cycling of sulfur in subduction zones: the geochemistry of sulfur in the Mariana Island Arc and back-arc trough. *Earth Planet. Sci. Lett.* 119, 477- 494.
- Alt, J., Burdett, A., 1992. Sulfur in deep sea sediments (Leg 129) and implications for cycling of sediments in subduction zones. Eds. Larson, R. L., Lancelot, Y., et al., 1992, *Proceedings of the Ocean Drilling Program, Scientific Results 129*, 283-495.
- Andersen, M.B., Elliott, T., Freymuth, H., Sims, K.W.W., Niu, Y., Kelley, K.A. 2015. The terrestrial uranium isotope cycle. *Nature* 517, 356-359.
- Barry, T.L., Pearce, J.A., Leat, P.T., Millar, I.L., le Roex, A.P., 2006. Hf isotope evidence: for selective mobility of high-field-strength elements in a subduction setting: South Sandwich Islands. *Earth Planet. Sci.* 252, 223–244.
- Behn, M. D. Kelemen, P.B., Hirth, G., Hacker, B.R., Massonne, H-J., 2011. Diapirs as the source of the sediment signature in arc lavas. *Nature Geosci.* 4, 641-646.
- Bezos, A., Escrig, S., Langmuir, C.H., Michael, P.J., Asimow, P.D., 2009. Origins of chemical diversity of back-arc basin basalts: a segment-scale study of the Eastern Lau Spreading Center. *J. Geophys. Res.—Solid Earth*, 114.
- Brown, J.L., Christy, A.G., Ellis, D.J., Arculus, R.J., 2007. Prograde sulphide metamorphism in blueschist and eclogite, New Caledonia, *J. Petrol.*, doi:10.1093/petrology/egu002.
- Canfield, D., 2004. The evolution of the earth surface sulfur reservoir. *American Journal of Science* 304, 839-861.
- Canil, D., 1999. The Ni in garnet geothermometer: calibration at natural abundances. *Contrib. Mineral. Petrol.* 136, 313-324.
- Carroll, M.R., and Rutherford, M.J., 1987. The stability of igneous anhydrite—Experimental results and implications for sulfur behavior in the 1982 El Chichon trachyandesite and other evolved magmas: *J. Petrol.* 28, 781–801.
- Collerson, K., Kamber, B., 1999. Evolution of the continents and atmosphere inferred from the Th-U-Nb systematics of the depleted mantle. *Science* 283, 1519-1523.
- Cooke, D. R., Hollings, P., Walshe, J. L. 2005. Giant porphyry deposits: Characteristics, distribution, and tectonic controls. *Econ. Geol.* 100, 801–818.
- Cooper, L.B., Ruscitto, D.M., Plank, T., Wallace, P.J., Syracuse, E.M., Manning, C. 2012, Global variations in H_2O/Ce : 1. Slab surface temperatures beneath volcanic arcs, *Geochem. Geophys. Geosys.* 13, doi:10.1029/2011GC003902
- De Hoog, J.C.M., B. E. Taylor, and M. J. van Bergen., 2001. Sulfur isotope systematics of basaltic lavas from Indonesia: implications for the sulfur cycle in subduction zones. *Earth Planet. Sci. Lett.* 189, 237-252.
- deMets, C. Gordon, G., Argus, D.F., 2010. Geologically current plate motions. *Geophys. J. Int.* 181, 1-80.

- Dril, S.I., Kuzmin, M.I., Tsipukova, S.S., Zonenshain, L.P., 1997. Geochemistry of basalts from the western Woodlark, Lau and Manus basins: implications for their petrogenesis and source rock compositions. *Mar. Geol.* 142, 57–83.
- England, P. C., Katz, R. F. 2010. Melting above the anhydrous solidus controls the location of volcanic arcs. *Nature* 467, 700–703.
- Evans., K.A., 2012. The redox budget of subduction zones. *Earth Sci. Rev.* 113,11-32.
- Evans, K., Powell, R., Holland, T., 2010. Internally consistent data for sulphur-bearing phases and application to the construction of pseudosections for mafic greenschist facies rocks in Na_2O - CaO - K_2O - FeO - MgO - Al_2O_3 - SiO_2 - CO_2 - O - S - H_2O . *J. Metam. Geol.* 28, 667–687.
- Farquhar, J., Wing, B.A., McKeegan, K.D., Harris, J.W., Cartigny, P., Thiemens, M.H. 2002. Mass independent S of inclusions in diamond and sulfur recycling in the early earth. *Science*, 298, 2369-2372..
- Falloon, T.J., Malahoff, A., Zonenshain, L.P., Bogdanov, Y., 1992. Petrology and geochemistry of back-arc basin basalts from lau basin spreading ridges at 15-degrees, 18-degrees and 19-degrees-S. *Mineral. Petrol.* 47, 1–35.
- Fellows, S.A., Canil, D., 2012. Experimental study of the partitioning of Cu during partial melting of Earth's mantle. *Earth Planet. Sci. Lett.* 337, 133-143.
- Fretzdorff, S., Livermore, R.A., Devey, C.W., Leat, P.T., Stoffers, P., 2002. Petrogenesis of the back-arc east Scotia Ridge, South Atlantic Ocean. *J. Petrol.* 43, 1435–1467.
- Frost, B.R., 1991. Introduction to oxygen fugacity and its petrologic importance. In: Lindsley, D.H. (ed) *Oxide minerals: petrologic and magnetic significance*. Mineral. Soc. Amer., *Rev. Mineral.* 25, 1-9.
- Gerya, T.V., Yuen, D.A., 2003. Rayleigh–Taylor instabilities from hydration and melting propel ‘cold plumes’ at subduction zones. *Earth Planet. Sci. Lett.* 212, 47–62.
- Gregory, M., 2006. Copper mobility in the Eastern Creek Volcanics, Mount Isa, Australia: evidence from laser ablation ICP-MS of iron-titanium oxides. *Miner. Deposita* 41, 691–711
- Harlov, D. 2012. The potential role of fluids during regional granulite facies dehydration of the crust. *Geosci Frontiers*, 3, 813-827.
- Hermann, J., Spandler, C.J., 2008. Sediment melts at sub-arc depths: an experimental study. *J. Petrol.* 49, 717–740.
- Hirschmann, M.M., Dasgupta, R.J., 2009. The H/C ratios of Earth's near-surface and deep reservoirs, and consequences for deep Earth volatile cycles. *Chem. Geol.* 262, 4–16.
- Higgins, J.A., Fischer, W.W., Schrag, J.P. 2009. Oxygenation of the ocean and sediments: Consequences for the seafloor carbonate factory. *Earth Planet. Sci. Lett.* 284, 25–33.
- Holland, T.J.B., 1990. Activities of components in omphacitic solid solutions: an application of Landau theory to mixtures, *Contrib. Mineral. Petrol.*, 105, 446-453.
- Holland, T.J.B., Powell, R., 1998. An internally consistent thermodynamic data set for phases of petrological interest. *J. Metam. Geol.* 16, 309–343.
- Jego, S., Dasgupta, R., 2013. Fluid-present melting of sulphide-bearing ocean-crust: Experimental constraints on the transport of sulfur from subducting slab to mantle wedge. *Geochim. Cosmochim. Acta* 110, 106-134.

- Jego, S., Dasgupta, R., 2014. The fate of sulfur during fluid-present melting of subduction basaltic crust at variable oxygen fugacity. *J. Petrol.*, 55, 1019-1050.
- Jenner, F.E., O'Neill, H.S., 2012. Analysis of 60 elements in 616 ocean floor basaltic glasses. *Geochem. Geophys. Geosyst.* 13, 11.
- Jenner, F.E., O'Neill, H.S., Arculus, R.J., Mavrogenes, J.A., 2010. The magnetite crisis in the evolutions of arc-related magmas and the initial concentration of Au, Ag and Cu. *J. Petrol.*, 51, 2445-2464.
- Jugo, P., 2009. Sulfur content at sulphide saturation in oxidized magmas. *Geology* 37, 415–418
- Jugo, P., Luth, R., Richards, J., 2005, Experimental data on the speciation of sulfur as a function of oxygen fugacity in basaltic melts: *Geochim. Cosmochim. Acta*, 69, 497–503.
- Kelley K.A., Cottrell, E. 2012. The influence of magmatic differentiation on the oxidation state of Fe in a basaltic arc magma. *Earth Planet. Sci. Lett.* 330, 109–121
- Lee, C.-T.A., Luffi, P., Chin, E.J., Bouchet, R., Dasgupta, R., Morton, D.M., Le Roux, V., Yin, Q., Jin, D., 2012. Copper systematics in arc magmas and implications for crust-mantle differentiation. *Science* 336, 64-68.
- Lee, C.-T.A., Luffi, P., Le Roux, V., Dasgupta, R., Albare' de, F., Leeman, W.P., 2010. The redox state of arc mantle using Zn/Fe systematics. *Nature* 468, 681-685.
- Lee, C.-T.A., Leeman, W.P., Canil, D., and Li, Z.A., 2005. Similar V/Sc systematics in MORBs and arc basalts : implications for the oxygen fugacities of their mantle source regions, *J. Petrol.* 46, 2313-2336.
- Malaspina, N., Poli, S., Fumagalli, P. 2009. The oxidation state of the metasomatized mantle wedge: Insights from C-O-H-bearing garnet peridotite, *J. Petrol.*, 50, 1533-1552.
- Mallik, A., Dasgupta, R., Tsuno, K., Nelson, J., 2016. Effects of water, depth and temperature on partial melting of mantle-wedge fluxed by hydrous sediment-melt in subduction zones. *Geochim. Cosmochim. Acta* 195, 226–243
- Marchall, H. R., Schumacher, J. C., 2012. Arc magmas sourced from melange diapirs in subduction zones. *Nature Geosci.* 5, 862-867.
- McInnes, B.I.A., McBride, J.S., Evans, N.J., Lambert, D.D., Andrew, A.S., 1999. Osmium isotope constraints on ore metal recycling in subduction zones. *Science* 286, 512-516.
- Mann, U., Schmidt, M.W., 2015. Melting of pelitic sediments at subarc depths: 1. Flux vs. fluid-absent melting and a parameterization of melt productivity. *Chem. Geol.* 404, 150–167.
- Miller, W.G.R., Holland, T.J.B., Gibson, S.A. 2016. Garnet and spinel oxybarometers: New internally consistent multi-equilibria models with applications to the oxidation state of the lithospheric mantle. *J. Petrol.*, 57, 1199-1220.
- Mungall, J.E., 2002. Roasting the mantle: Slab melting and the genesis of major Au and Au-rich deposits. *Geology* 30, 915-918.
- Parkinson, I.J., Arculus, R.J., 1999. The redox state of subduction zones: insights from arc-peridotites. *Chem. Geol.* 160, 409-423.
- Patino, L.C., Carr, M.J., Feigenson, M.D., 2000. Local and regional variations in Central American arc lavas controlled by variations in subducted sediment input. *Contrib. Mineral. Petrol.* 138, 265.

- Patten, C.G.C, Pitcairn, I.K., Teagle, D.A.H., Harris, M., 2016. Mobility of Au and related elements during the hydrothermal alteration of the oceanic crust: implications for the sources of metals in VMS deposits. *Miner. Deposita* 51, 179–200
- Pearce, J.A., Stern, R.J., Bloomer, S.H., Fryer, P., 2005. Geochemical mapping of the Mariana arc-basin system: implications for the nature and distribution of subduction components. *Geochem. Geophys. Geosyst.*, 6.
- Penniston-Dorland, S.C., Kohn, M., Manning, C., 2015. The global range of subduction zone thermal structures from exhumed blueschists and eclogites: Rocks are hotter than models. *Earth Planet. Sci. Lett.* 428, 243–254.
- Plank, T., 2005. Constraints from thorium/lanthanum on sediment recycling at subduction zones and the evolution of the continents. *J. Petrol.* 46, 921–944.
- Plank, T., Langmuir, C.H., 1993. Tracing trace-elements from sediment input to volcanic output at subduction zones. *Nature* 362, 739–743.
- Plank, T., Langmuir, C.H., 1998. The chemical composition of subducting sediment and its consequences for the crust and mantle. *Chem. Geol.* 145, 325–394.
- Plank, T., Balzer, V., Carr, M. 2002. Nicaraguan volcanoes record paleoceanographic changes accompanying closure of the Panama gateway. *Geology* 30, 1087–1090.
- Pons, M.-L., Debret, B., Bouilhol, P., Williams, H., 2016. Zinc isotope evidence for sulfate-rich fluid transfer across subduction zones. *Nature* DOI: [10.1038/ncomms13794](https://doi.org/10.1038/ncomms13794)
- Prouteau, G., Scaillet, B., 2013. Experimental constraints on sulphur behaviour in subduction zones: Implications for TTG and adakite production and the global sulphur cycle since the Archean. *J. Petrol.* 54, 183–213.
- Ridgwell, A., Zeebe, R.A. 2005. The role of the global carbonate cycle in the regulation and evolution of the Earth system. *Earth Planet. Sci. Lett.* 234, 299–315.
- Scaillet, B., Clemente, B., Evans, B.W. & Pichavant, M. (1998). Redox control of sulfur degassing in silicic magmas. *J. Geophys. Res.* 103, 23937–23949.
- Schmidt, M.W., 2015. Melting of pelitic sediments at subarc depths: 2. Melt chemistry, viscosities and a parameterization of melt composition. *Chem. Geol.* 404, 168–182.
- Shervais, J.V., 1982. Ti-V plots and the petrogenesis of modern and ophiolitic lavas. *Earth Planet. Sci. Lett.* 59, 101–118.
- Shu, X-J., Lee, C-T.A. 2015. Sulfur determination by laser ablation high resolution magnetic sector ICP-MS applied to glasses, aphyric lavas, and micro-laminated sediments. *Chinese J. Geochem.* 34, 273–288.
- Skora, S., Blundy, J., 2010. High-pressure hydrous phase relations of radiolarian clay and implications for the involvement of subducted sediment in arc magmatism. *J. Petrol.* 51, 2211–2243.
- Skora, S., Blundy, J., Brooker, R., 2015. Hydrous phase relations and trace element partitioning behaviour in calcareous sediments at subduction zone conditions. *J. Petrol.* 56, 953–980.
- Spandler, C.J., Yaxley, G., Green, D.H., Scott, D., 2010. Experimental phase and melting relations of metapelite in the upper mantle: implications for the petrogenesis of intraplate magmas. *Contrib. Mineral. Petrol.* 160, 569–589.
- Syracuse, E.M., van Keken, P.E., Abers, G.A., 2010. The global range of subduction zone thermal models. *Phys. Earth Planet. Inter.* 183, 73–90.

- Tera, F., Brown, L., Morris, J., Sacks, I.S., Klein, J., and Middleton, R., 1986. Sediment incorporation in island-arc magmas: Inferences from ^{10}Be : *Geochim. Cosmochim. Acta* 50, 535–550.
- Tomkins, A., Evans, K.A., 2015. Separate zones of sulphate and sulphide release from subducted mafic oceanic crust. *Earth Planet. Sci. Lett.* 428, 73–83.
- Tsuno, K., Dasgupta, R., 2011. Melting phase relation of nominally anhydrous, carbonated pelitic-eclogite at 2.5–3.0 GPa and deep cycling of sedimentary carbon. *Contrib. Mineral. Petrol.* 161, 743–763.
- Ulmer, P., Luth, R.W., 1990. The graphite-COH fluid equilibrium in P, T, f_{O_2} space. *Contrib. Mineral. Petrol.* 106, 265–272.
- van Keken, P.E., Hacker, B.R., Syracuse, E.M., Abers, G.A., 2011. Subduction factory: 4. Depth-dependent flux of H_2O from subducting slabs worldwide. *J. Geophys. Res.* 116. <http://dx.doi.org/10.1029/2010JB007922>.
- Wallace, P.J. 2005. Volatiles in subduction zone magmas: concentrations and uxes based on melt inclusion and volcanic gas data. *J. Volc. Geotherm. Res.* 140, 217–240.
- Woodland, A. , Kornprobst, J., Tabit, A. 2006. Ferric iron in orogenic lherzolite massifs and controls of oxygen fugacity in the upper mantle, *Lithos*, 89, 222–241.
- Wood, B.J. 1979. Activity-composition relationships in $\text{Ca}(\text{Mg,Fe})\text{Si}_2\text{O}_6$ - $\text{CaAl}_2\text{SiO}_6$ clinopyroxene solid solutions. *Am. J. Sci.*, 279, 854–875.

Figure Captions

Figure 1 – Bulk compositions (wt% $\text{SiO}_2 + \text{Al}_2\text{O}_3$, Cu/Sc, wt.% CO_2 and X_{Ca} = molar $\text{Ca}/(\text{Ca} + \text{Mg} + \text{Fe})$) derived for composite marine sediment columns at trenches of various convergent margins (Plank and Langmuir, 1988). Note the spectrum of convergent margin sediments varies from pelitic to carbonate-rich, with no change on bulk Cu/Sc. These data are compared with those for starting materials in experiments on melting of sediments at subduction zone P-T conditions (Spandler et al., 2007; Hermann and Spandler, 2008; Tomsen and Schmidt, 2008; Skora and Blundy, 2010; Skora et al., 2015; Tsuno and Dasgupta, 2011; Prouteau and Scaillet, 2013; Mann and Schmidt, 2015).

Figure 2 - Comparison of X_{Ca} (= molar $\text{Ca}/(\text{Ca} + \text{Mg} + \text{Fe})$) of garnet and X_{Hed} of clinopyroxene with that of the starting material in experiments on slab sediment bulk compositions over a range of P-T conditions (2 – 5 GPa, 700 – 1100°C). Note the strong correlation of garnet X_{Ca} with bulk composition, but lesser correlation for X_{Hed} in clinopyroxene (which depends mostly on T). Sources for experimental data as given in Figure 1.

Figure 3 - Difference in measured $\log f\text{O}_2$ values and those calculated using the GAP method (reaction [1] in text) for experiments saturating in clinopyroxene+garnet and either anhydrite, pyrrhotite or both. Mineral chemical data were from experiments between 2 and 3 GPa on bulk compositions of metabasalt (Jego and Dasgupta, 2013; 2014) and metapelite (Prouteau and Scaillet, 2013).

Figure 4 – Pressure and temperatures (open circles) recorded by blueschist and eclogites from exhumed subduction-related metamorphic terrains (Penniston-Dorland et al, 2015) compared with a model P-T trajectory calculated for the top of a hot young slab (thick green line - van Keken et al., 2011). Simple fits through the middle ('warm') and hottest ('hot') temperatures of the blueschist/eclogite data are given, and were used in the sulphide-sulphate buffer calculations in text and plotted Figure 5. Triangles are the P-T

conditions under which sediment melting experiments have been performed (data sources given in Figure 1 caption).

Figure 5 – The $\log fO_2$ of sulphide-sulphate (SSO) buffers in subducted oceanic crust (reactions [1-4] in text) plotted relative to that of the surrounding mantle (assumed to be at the FMQ buffer - after Frost, 1991) as a function of depth for various P-T trajectories of subduction. Sulphide is stable in subducted sediment at depths where the fO_2 of its given SSO buffer is greater than of the peridotitic mantle (i.e. $\Delta FMQ > 0$). Beyond that depth, the fO_2 of a SSO buffer is less than that of the peridotitic mantle ($\Delta FMQ < 0$) and sulphate is stable in a given bulk sediment composition (blue shaded field). The effects of bulk compositions of oceanic sediments are expressed as X_{Ca} of garnet or X_{Hed} clinopyroxene (0.1 to 0.5) in the SSO buffer reaction. The P-T trajectories for subducted crust (vanKeken, warm, hot) in the various panels are shown and described in Figure 4. Horizontal orange stippled field shows the range of depths to the slab measured beneath the volcanic fronts of modern arcs (England and Katz, 2010). (a) CAP and GAP buffers for two different X_{Ca} in the sediment (0.1 and 0.5) on a ‘vanKeken’ P-T trajectory for the slab; (b) CAP and GAP buffers for X_{Ca} in the sediment (0.1 and 0.5) on a ‘warm’ slab P-T trajectory; (c) CAP buffer with constant sediment composition ($X_{Ca}=0.5$) along three different P-T trajectories for the slab (vanKeken, warm, and hot); (d) CAP and CAPY buffers on a ‘vanKeken’ P-T trajectory for the slab showing effect of the different sulphide identity (Py vs. Po) on depth for sulphide stability.

Figure 6 - Capsule configuration for the sediment melting experiments (Table 1). Oxidized conditions used a starting material (SM) placed inside of two gold capsules; one containing S as S^{2-} (in pyrite), and one as S^{6+} (in anhydrite). The two capsules were surrounded by gibbsite ($Al(OH_3)$) to ensure H_2O saturation and prevent fluid loss through the Au capsule. Reduced experiments were carried out under the same configuration but with graphite (C) powder added both to the gold capsules as well as mixed with the surrounding gibbsite.

Figure 7 – Back scattered electron images of experimental run products. Scale bar in lower right. (a) Experiment p403 (GMan starting composition) with S added as disseminated anhydrite containing clinopyroxene (cpx), K-feldspar (Ksp), phengite (Phen), and melt (gl) as well as fluid bubble (V). (b) Run product for p409py (TSC starting composition) containing clinopyroxene (cpx), pyrrhotite (Po), calcite melt (Cc), titanite (Ttn) and melt (gl).

Figure 8 - Sulfur, Cu, Zn, As, Mo, Pb and Sb concentrations of experimental melts vs. $\log fO_2$ of the experiments [at all temperatures](#) expressed relative to the FMQ buffer. Representative uncertainties (1σ) are shown for only one element for clarity. Note the several-fold enrichment of chalcophile elements in melts [when saturated in anhydrite \(filled symbols\) relative to those saturated in pyrrhotite \(open symbols\)](#). The $\log fO_2$ (in ΔFMQ format) used for this plot were calculated using the CAP and/or GAP buffers assemblages applied to experimental run products that saturate in these assemblages. [The \$\log fO_2\$ can only be regarded as minima or maxima \(arrows\) because they saturated in either pyrrhotite or anhydrite only, never both \(see Table 2 and text for details\).](#)

Figure 9 – Concentrations of trace elements in sediment melts normalized to their concentrations in the starting material. Note similar behavior of all elements in sulphate-saturated experiments (blue lines), but marked depletion in chalcophiles Cu, As, Zn, Sb and Pb relative to lithophiles (Sc, Nb, Ba, La, Ce, Yb, Th, U) for pyrrhotite-saturated melts (red lines). Also shown are key element ratios applied in sources for arc magmatism. Note order of magnitude higher Cu/Sc observed for sulfate-saturated melts.

Figure 10 – Plot of Cu/Sc for Miocene lavas (solid triangles with $< 60\%SiO_2$) erupted in the Nicaraguan segment of the Central American Arc relative to their distance to the modern trench. These are compared with the wt% $CaCO_3$ in sediments of various ages drilled on the subducting Cocos plate (solid circles). The ages of the sediments (20 to 0.45 Ma) are converted to their distance relative to the modern trench, assuming a plate velocity of 85 mm/y (deMets et al., 2010). Data for Nicaraguan volcanic rocks and Cocos plate sediments are from Plank et al (2002). Large diamond shows the mean and one

standard error of Cu/Sc in Quaternary and younger arc lavas from Central America
compiled in E-Appendix B and C (note scale adjusted, real distance from modern trench
= 100 km).

Figure 11 – Plot of mean Cu/Sc compiled for lavas containing < 60 wt% SiO₂ in modern
arcs compared with X_{Ca} of convergent margin sedimentary sections for which data are
available (Plank and Langmuir, 1998). Uncertainties in Cu/Sc are given as one standard
error of the mean, and those shown for X_{Ca} of the sedimentary section are assumed to be
±20% (E-Appendix B, Plank and Langmuir, 1998). The data are fitted to an equation of
the same form describing the S speciation in silicate melts ($r^2 = 0.97$, see text). Data
sources are given in an E-Appendix B.

Figure 12 – Strip charts comparing Cu/Sc for MORB glasses, back-arc basalt glasses
(ARC GL), arc lavas with < 60wt.% SiO₂ (ARC WR) and Archean ‘arc’ basalts with >
6wt.% MgO (ARCHEAN). The Cu/Sc in whole rocks and submarine glasses from
modern arcs is significantly higher, on average ($t_{4023} = -16.80$, $p < 0.0001$, $t_{147} = -5.52$,
 $p < 0.0001$, respectively), and more variable than that of MORB. In contrast, the mean
Cu/Sc of Archean arc basalts is similar to MORB, but significantly lower than that of
modern arc whole rocks or glasses ($t_{356} = -5.03$, $p < 0.0001$). Data sources are: MORB -
Jenner and O’Neill (2012); ARG GL – Falloon et al. (1992), Pearce et al. (2005), Dril et
al. (1997), Barry et al. (2006), Fretzdorff et al. (2002), Bezos et al. (2009); ARC WR –
see E-Appendix B; ARCHEAN - see E-Appendix B